Adipose-derived exosomal miR-421 targets CBX7 and promotes metastatic potential in ovarian cancer cells

Yi Zhang[1*], Roslyn Tedja[2*], Michael Millman[1], Terrence Wong[2], Alexandra Fox[2], Hussein Chehade[2], Meyer Gershater[2], Nicholas Adzibolosu[2], Radhika Gogoi[2], Matthew Anderson[3], Thomas Rutherford[3], Zhenggang Zhang[1], Michael Chopp[1,4], Gil Mor[2], Ayesha B. Alvero[2]

[1] Neurology, Henry Ford Health, Detroit, MI;

[2] C.S. Mott Center for Human Growth and Development, Department of Obstetrics and Gynecology, Wayne State University, Detroit, MI;

[3] Department of Obstetrics and Gynecology, University of South Florida, Tampa, FL;

[4] Department of Physics, Oakland University, Rochester, MI

* Authors contributed equally

Running title: Adipose-derived exosomal miRNA and ovarian cancer cells

Corresponding authors:

Ayesha B. Alvero, MD, MSc
C.S. Mott Center for Human Growth and Development
Department of Obstetrics and Gynecology
Wayne State University
275 E. Hancock St.
Detroit, MI 48201
(313) 577-1794
ayesha.alvero@wayne.edu

Yi Zhang, PhD
Neurology
Henry Ford Health System
2799 W Grand Blvd.
Detroit, MI 48202
(313) 916-8954
YZHANG3@hfhs.org

Abstract

Background: Chromobox protein homolog 7 (CBX7), a member of the Polycomb repressor complex, is a potent epigenetic regulator and gene silencer. Our group has previously reported that CBX7 functions as a tumor suppressor in ovarian cancer cells and its loss accelerated formation of carcinomatosis and drove tumor progression in an ovarian cancer mouse model. The goal of this study is to identify specific signaling pathways in the ovarian tumor microenvironment that down-regulate CBX7. Given that adipocytes are an integral component of the peritoneal cavity and the ovarian tumor microenvironment, we hypothesize that the adipose microenvironment is an important regulator of CBX7 expression. Results: Using conditioned media from human omental explants, we found that adipose-derived exosomes mediate CBX7 downregulation and enhance migratory potential of human ovarian cancer cells. Further, we identified adipose-derived exosomal miR-421 as a novel regulator of CBX7 expression and the main effector that downregulates CBX7. Conclusion: In this study, we identified miR-421 as a specific signaling pathway in the ovarian tumor microenvironment that can downregulate CBX7 to induce epigenetic change in OC cells, which can drive disease progression. These findings suggest that targeting exosomal miR-421 may curtail ovarian cancer progression.

Background

Cancer progression requires continuous acquisition of functions that support and increase aggressiveness and malignancy. Initial driver mutations, which can initiate malignant transformation are eventually followed by the creation of a pro- tumor microenvironment as cancer cells “educate” its surrounding stroma. In advanced stages, fibroblasts, immune cells, adipocytes, within this microenvironment would have been reprogrammed to primarily function as supporters of cancer growth and metastasis (1-3).

Adipose tissue is a central component of the cancer microenvironment (4), and is made up mostly of adipocytes and to a lesser extent, endothelial cells, and macrophages (5). Factors secreted by adipocytes as well as direct adipocyte-cancer cell interaction have been shown to support tumor progression in various cancer types including, breast, ovarian, prostate, and colon cancers (6-10).

Ovarian cancer (OC) is the most lethal of all gynecological malignancies and accounts for about 12,000 deaths annually (11). OC rarely metastasizes via the hematogeneous route, and almost exclusively metastasizes via shedding into the peritoneal cavity (12-14). Adipose-rich tissues within the abdomen are preferential sites for OC metastasis (15-18) (10, 17-19) and includes areas such as the omentum, mesosalphingeal/mesoovarian adipose, and adipose niches in the mesentery. Adipocytes have been shown to promote OC progression by providing fatty acids as an energy source to sustain rapid metastatic growth (20-22). In addition, adipocytes have been shown to enhance OC metastasis through secretion of chemotactic factors such as IL-8 and to promote chemoresistance by activating the Akt pathway (23) and upregulating the pro-survival protein Bclxl (24).

Chromobox protein 7 (CBX7) is a member of the Polycomb repressor complex 1 (PRC1). PRC1, and together with PRC2, are epigenetic regulators that induce histone modifications leading to repression of transcription (25-29). As part of PRC1, CBX7 is able to inhibit gene expression by binding to tri-methylated lysine 27 on histone 3 (H3K27me3) and inducing the monoubiquitination of lysine 119 on nearby histone 2A (H2Aub1) (30-33). CBX7 has been described as an oncogene, which is able to cooperate with c-Myc to induce aggressiveness in lymphomas (26) and contribute in the immortalization of fibroblasts (34). In other studies however, CBX7 has been described as a tumor suppressor and its downregulation has been correlated with aggressiveness and poor prognosis in thyroid, breast and colon cancers (35-38). Specifically, for OC, our previous work has demonstrated that the loss of CBX7 is correlated with enhanced metastatic potential and reduced patient survival (39). Mechanistically, CBX7 is able to achieve this by competing with Twist1 for binding to the E-box (39). As a result, Twist1, which is a master regulator of mesenchymal function cannot fully achieve its transcriptional role. Deletion of CBX7 using CRISPR/Cas9 relieves this inhibition allowing Twist1 to function and conferring enhanced metastatic potential to OC cells (39).

Exosomes are a subtype of small extracellular vesicles (EVs), which are released from cells into the extracellular space. They range in size from ~30 to 150nm in diameter and carry various cargoes such as proteins, lipids, and nucleic acids, which reflect the composition of its cellular origin(40-42). In the tumor microenvironment, exosomes are secreted by cancer cells, infiltrating immune cells, endothelial cells, and cancer-associated fibroblasts (43-46) , and mediate intercellular communication consequently contributing to various processes required for tumor progression such as cell proliferation, angiogenesis, and enhanced metastatic potential (43, 47-49).

Having demonstrated the significant impact of CBX7 loss on OC progression (39), we sought in this study to identify specific mechanisms within the ovarian tumor microenvironment that can regulate its expression. We report that adipose-derived exosomal microRNA-421 (miR-421) regulates CBX7 expression and function confers cancer cells with metastatic potential.

Results

Adipose-derived factors downregulate CBX7 and enhance migratory capacity in OC cells

Our group previously reported that CBX7 functions as a tumor suppressor in OC and its loss enhances metastasis in an OC xenograft model (39). In addition, *in vitro* migration through trans-well insert is also significantly augmented in OC cells upon CRISPR/Cas9-mediated knocked-out (KO) of CBX7 (Supp. Fig. 1). Thus, we hypothesize that factors secreted by the tumor microenvironment may be responsible for the regulation of CBX7 expression and function. Given the known significance of the adipose niche in OC progression, we posited that adipocytes may affect CBX7 expression. As such, we collected adipose conditioned media (ACM) from a human omental explant isolated from a female patient who underwent laparoscopic surgery for a benign gynecological condition and treated a panel of human OC cells. After 5 days of treatment, we observed that ACM are able to down-regulate CBX7 in all OC cells tested (Fig. 1A).

Interestingly, ACM induced morphological changes characteristic of fibroblastic morphology (Fig.1B). Characterization of markers associated with epithelial mesenchymal transition (EMT) following treatment with ACM showed downregulation of CBX7, upregulation of the mesenchymal marker FOXC2, and maintained expression of Twist1 and Vimentin (Fig. 1C).

To evaluate if ACM is able to enhance functions that support metastatic potential, we collected OC cells after treatment with ACM and performed the trans-well migration assay. We observed

that pre-treatment with ACM significantly enhanced *in vitro* migratory capacity compared to no treatment (Fig. 1D). Since the migration assay was performed in the absence of ACM, these results demonstrate that pre-treatment with ACM is able to confer cell autonomous mechanisms that can support metastatic potential. These results also show that ACM treatment recapitulates the enhanced migratory potential observed in CBX7 KO OC cells.

Characterization of adipose-derived exosomes

Further characterization of CBX7 status after treatment with ACM showed that the down-regulation of CBX7 protein was not associated with a decrease in CBX7 mRNA (Supp. Fig. 2) suggesting a possible post-transcriptional mechanism. miRNAs are short non-coding RNAs that function in the post-transcriptional control of gene expression (50). miRNAs provide a specific sequence that recruits ribonucleoprotein (RNP) complex to the 3' untranslated region (3'UTR) of target messenger RNAs (mRNAs) (51-53). The binding of miRNA-RNP complex to their target mRNAs results in mRNA degradation or translational repression and therefore downregulation of protein expression (54). We hypothesized that ACM downregulates CBX7 through its miRNA content. Since miRNAs are packaged and protected in EVs such as exosomes(55-57), we further hypothesized that these miRNAs may be carried in exosomes. Thus, we collected a new set of ACM obtained from 6 different patient omenta (Table 1) and performed differential ultracentrifugation to isolate exosomes. Characterization of the isolates with NanoSight showed homogeneous exosome preparations with average size of 100 nm (Fig. 2A). TEM analysis showed typical exosomal morphology of double layered cup-shaped membrane structure (Fig. 2B) and Western blot analysis showed the presence of tetraspanin markers, CD63 and CD9, and the absence of the endoplasmic reticulum marker, calnexin(58) (Fig. 2C) demonstrating that the collected particles are exosome-like small EVs.

The human omentum is primarily composed of adipocytes and immune cells within “milky spots” (59). To determine the cellular origin of the isolated exosomes, we utilized the ExoView platform to assay exosomal membrane proteins, which maintain the same characteristics as the cell of origin (60-62). Thus, we captured the exosomes using CD63, CD81 and CD9 antibodies and utilized CD36 and CD11b to identify the adipocyte and macrophage exosomal cell sources, respectively. Our results show significantly higher percentage of exosomes carrying the adipocyte marker, CD36 than the macrophage marker, CD11b (Fig. 2D and 2E) ,demonstrating that majority of the isolated exosomes from the ACM originate from adipocytes.

Adipose-derived exosomes are sufficient to downregulate CBX7

To demonstrate that the isolated ACM-derived exosomes can be internalized by OC cells, we labelled the exosomes by their cargo RNAs with green fluorescence (GF-exosomes)(63, 64) and exposed them to mCherry-labeled OC cells. Microscopic analysis showed co-localization of GF-exosomes and mCherry OC cells, demonstrating the internalization of the labelled exosomes by the OC cells (Fig. 3A) and the putative delivery of their contents.

We next determined the effect of ACM-derived exosomes on CBX7 expression. Interestingly, of the 6 exosome preparations tested, only 4 were able to down-regulate CBX7 (Fig. 3B). Patient 652, 626, 628 and 568 consistently down-regulated CBX7 compared to no treatment Control although only 652 reached statistical significance. To demonstrate that the effect on CBX7 is an exclusive property of the exosomes, we treated OC cells with ACM, isolated exosomes, or exosome-depleted ACM. Both ACM and isolated exosomes were able to decrease CBX7 expression, but this effect was lost in the exosome-depleted ACM (Fig. 3C and 3D). Finally, to further support that the observed decrease in CBX7 is due to exosome cargo, we treated OC cells with exosomes in the presence or absence of the endocytosis inhibitor, Nystatin. We observed that pre-treatment with Nystatin abrogated the effect of exosomes on CBX7 (Fig. 3C). Taken

182 together, our results demonstrate that adipose-derived exosomes can down-regulate CBX7 in OC
183 cells.
184
185 *Adipose-derived exosomal miR-421 targets CBX7 in OC cells*
186 We next sought the determine the signaling pathway responsible for the observed changes in
187 CBX7 expression. In keeping with the hypothesis that this may be secondary to exosomal miRNA
188 cargo we utilized mirTarBase (https://mirtarbase.cuhk.edu.cn and TargetScanHuman
189 (https://targetscan.org/) to generate a list of miRNAs predicted to target CBX7 (Table 2 and Table
190 3). We then cross-referenced this to published lists of exosomal miRNA that are known to be
191 almost exclusively derived from adipocytes. The first list came from the comparison of circulating
192 exosomal miRNA between AdicerKO mice (mice specifically lacking Dicer in adipose tissue
193 generated using Cre-*lox* gene recombination) and wild-type controls (65). The second list came
194 from the same study and a comparison of circulating exosomal miRNA between patients with
195 congenital lipodystrophy (CGL) and healthy controls (65). Venn diagram analysis identified only
196 one common miRNA from this list, which is miR-421 (Fig. 4A).
197
198 We then proceeded to determine if miR-421 contributes to the exosomal signal that leads to ACM-
199 induced CBX7 downregulation in OC cells. Thus, we treated OC cells with ACM derived
200 exosomes in the presence or absence of anti-miR-421 or Control anti-miR. Our results show that
201 the anti-miR-421, but not Control anti-miR, abrogated the effect of exosomes on CBX7 (Fig. 4B).
202 In addition, we treated OC cells with miR-421 mimic and observed that transient expression of
203 miR-421 mimic is sufficient to induce downregulation of CBX7 (Fig. 4C).
204
205 To conclusively demonstrate that CBX7 is a direct target of miR-421, we constructed a luciferase
206 reporter upstream of CBX7's 3' UTR (pCBX7; Fig. 4D). Co-transfection of pCBX7 reporter in
207 human OC cells with miR-421 resulted in a significant decrease in luciferase activity compared to

pCBX7 reporter alone and pCBX7 co-transfected with Negative Control miRNA (Fig. 4E). This effect of miR-421 is specific to this sequence on CBX7's 3'UTR as mutation of this sequence (pCBX7mut; Fig. 4D) abrogated the ability of miR-421 to decrease the luciferase signal (Fig. 4E). Collectively, these results demonstrate that the CBX7 gene is the direct target of miR-421 in OC cells.

miR-421 is detectable in adipose-derived exosomes

In utilizing exosome preparations from 6 individual patients, we observed that only 4 of the 6 samples downregulated CBX7 (Fig. 3). Our final objective is to determine if we can detect miR-421 in the adipose-derived exosomes. We were able to detect mir-421 in our exosome preparations and in addition, we observed that exosomes that were able to induce CBX7 downregulation contained relatively increased levels of miR-421 (Fig. 4F). Taken together, our results show that miR-421 is a direct regulator of CBX7, and that adipose-derived exosomes are an important source of miR-421 in the ovarian tumor microenvironment.

Discussion

We report a novel mechanism by which the adipose microenvironment can alter the phenotype of OC cells. In this study, we identified the existence of a miR-421/CBX7 axis that can lead to the downregulation of CBX7, a major component of the PRC. We demonstrate that the adipose niche is an important source of miR-421 and that it is packaged in exosomes. Our data demonstrate that adipose-derived exosomal miR-421 can function as an epigenetic regulator in OC cells by regulating CBX7.

Previously, we reported that CBX7 has tumor suppressor functions (39). Expression of CBX7 maintains OC epithelial phenotype by inhibiting mesenchymal triggers such as Twist1 (39).

Suppression of CBX7 in OC cells is associated with mesenchymal transformation and acquisition of metastatic potential. In this study we investigated the potential factors and sources responsible for the regulation of CBX7 expression and function, and consequently, the progression of OC. The findings reported here, highlight the contribution of the adipose niche in OC tumor progression.

CBX7 performs its gene-silencing function by modifying DNA-associated histones (25-29). As such, the genes repressed by CBX7, and hence the PRC complex, changes depending on cell state. As we previously reported, specifically for ovarian cancer, the expression of CBX7 alone is not predictive of survival (39). However, when used as a biomarker in conjunction Twist1, the absence of CBX7 in Twist1-positive ovarian cancer cells confers worse outcomes (ref). Whether or not CBX7 has a role in the initiation of ovarian cancer, such as exertion of pro-tumorigenic functions in normal ovarian surface epithelial cells or normal fallopian tube epithelial cells remains to be characterized. Nevertheless, our studies have shown that CBX7 is a major regulator of ovarian cancer progression (39) and that it can be regulated by factors secreted from adipocytes.

Secreted factors from the omentum have been shown to act as chemotactic factors that attract OC cells to this organ. Upon arrival, omental adipocytes have been shown to modulate OC cancer proliferation, metabolism, and response to chemotherapy(9, 66, 67). Given that OC mostly metastasizes via the trans-coelomic route and is mainly contained within the peritoneal cavity, the demonstration that adipose-derived exosomal miRNA can modulate epigenetic regulators in OC cells show that these cancer cells do not need to be in direct contact with adipocytes and can be located anywhere in the peritoneal cavity to be re-programmed by this microenvironment.

Although not fully characterized, selective loading of distinct molecules into exosomes is tightly regulated and does not occur randomly (68). Previous studies comparing intracellular versus

exosomal miRNA content for instance, showed that some miRNAs are selectively packaged into exosomes , while specific miRNAs are actively excluded. This is true in both normal cells such as astrocytes and neurons (69) as well as cancer cells. In laryngeal squamous cell carcinoma for instance, miR-1246, miR-1290, miR-335-5p, miR-127-3p and miR-122-5p are selectively packaged in exosomes, while miR-4521, miR-4483, miR-30b-5p, miR-29b-3p and miR-374b-5p are selectively retained in the cell (70). A recent study has demonstrated that miRNA sequence motifs determine whether they are favorably sorted into exosomes or retained in cells(71). It has been postulated that this sorting may reflect the pro-survival benefits of the retained miRNAs to the cancer cells, while secreted miRNAs may provide benefit by regulating the tumor microenvironment. Still, this sorting mechanism is highly dynamic and can change depending on cellular state (72). It is therefore not surprising that not all ACMs tested were able to downregulate CBX7. It is tempting to speculate that pre-existing metabolic-associated risk factors known to significantly impact OC risk and survival such as body mass index(73) , diabetes(74) , or high-fat diet (75) can affect miRNA sorting into adipose-derived exosomes. Other conditions such as aging(76), menopause(77), and hormone replacement therapy(78) have been shown to affect the repertoire of circulating miRNAs. Moreover, the intracellular destination and processing pathways of exosomes after uptake by recipient cells are highly heterogeneous, which lead distinct biological activities in recipient cells (79). These correlations are currently under investigation in our lab.

Although free miRNAs can be detected in the circulation, the protective effect of exosomal membranes contribute to its stability (68). Indeed, exosomal miRNAs have been proposed as biomarkers for OC (80, 81). And, adipocyte derived exosomes have been successfully detected in blood (65). The demonstration that adipose-derived exosomal mir-421 can directly impact OC metastatic potential suggests the possible utility of exosomal miR-421 as a marker to identify patients needing closer follow up for recurrence.

Conclusions

In conclusion, in this study we demonstrate that adipose-derived exosomal miR-421 within the tumor microenvironment downregulates CBX7 and consequently may enhance OC metastatic potential. These findings suggest that miR-421 is a molecular therapeutic target and a biomarker in OC patients.

Materials and Methods

Cell lines and culture conditions

OVCA432 (RRID:CVCL_3769) and OVCAR3 (RRID:CVCL_DH37) were obtained from ATCC (Manassas, VA) and cultured as instructed. The isolation and characterization of R182 and OCSC1-F2 have been previously reported (10, 82-85). These cells were cultured in RPMI1640 media supplemented with 10% FBS and 1% Pen/Step. Cells were grown in standard cell culture condition at 37°C with 5% CO_2. For all experiments, cells were kept below 80% confluence. Mycoplasma testing was performed every 6 months and short tandem repeat (STR) profiling was done annually. Cells were used within 6 passages between experiments.

Reagents and antibodies

Nystatin was purchased from MilliporeSigma (Cat. No. 1400-61-9). Mirvana miRNA mimic hsa-miR-421 (Cat. No. 4464066) was purchased from Thermo Scientific, Waltham, MA. miRIDIAN hsa-mir-421 hairpin inhibitor (Cat. No. IH-300996-03) was purchased from Horizon Discovery, (Waterbeach, UK). Lipofectamine RNAiMAX was purchased from Invitrogen (Waltham, MA). Antibodies used were anti-CBX7 (RRID:AB_726005; 1:1000, Cat. No. ab21873, Abcam, Cambridge, UK), anti-β-actin (RRID:AB_2923704; 1:1000, Cat. No. 81115-1-RR, Proteintech,

Rosemont, IL), anti-FOXC2 (RRID:AB_2798074;1:1000, Cat. No. 12974, Cell Signaling Technology, Danvers, MA), anti-Twist1 (RRID:AB_1130910; 1:500, Cat. No. CS-81417, Santa Cruz Biotechnology), anti-Vimentin (RRID:AB_10695459; 1:1000, Cat. No. 5741, Cell Signaling Technology, Danvers, MA), anti-GAPDH (RRID:AB_1078991; 1:10000, Cat. No. G8795, Sigma-Aldrich, St. Louis, MO).

Human subjects and generation of adipose conditioned media

Sample collection was obtained with informed consent with prior approval from Karmanos Cancer Center and the University of South Florida IRB. Samples were consecutively collected from patients undergoing laparoscopic or open surgery for a benign or malignant gynecological condition irrespective of diagnosis or age. Upon receipt from the clinic, omentum tissues were minced with sterile razor blades and approximately 0.5 g of minced tissue was cultured per 100 mm tissue culture dish in 10 mL DMEM/F12 media supplemented with 1% exosome-depleted FBS (EXO-FBS-250A-1, System Biosciences, Palo Alto, CA). The following day, growth media were refreshed. and cell-free conditioned media were collected by centrifugation. Adipose tissue conditioned media (ACM) were stored at -80°C.

Isolation of exosomes

Exosomes were isolated from the ACM via differential ultracentrifugation according to our published protocol (86, 87). Briefly, ACM was filtered through a 0.22 μm filter (MilliporeSigma, Burlington, MA) to remove all dead cells and large debris. The supernatant was then centrifugated at 10,000×g for 30 min followed by ultracentrifugation at 100,000×g (Optima XE-100 Ultracentrifuge, Beckman Coulter, Brea, CA) for 2 h. The resulting precipitate was re-suspended in phosphate-buffered saline (PBS) and used immediately or stored at 4°C.

Characterization of exosomes

Collected particles were characterized according to MISEV 2018 guidelines (88). Briefly, the concentration and size distribution of exosomes were determined by Nanoparticle Tracking Analysis (NTA, NanoSight NSr300, Malvern, UK), according to our published protocol (86, 87). The ultrastructural morphology and the expression of exosomal markers were examined by transmission electron microscopy (TEM, JEOL, JEM 1400) and Western blotting, respectively (86, 87).

ExoView single-EV profiling assay

After passing through 0.22 μm filter (MilliporeSigma, Burlington, MA), ACM were incubated with ExoView tetraspanin chips. Exosomes in ACM were captured by antibodies pre-coated on the chips, and against exosomal tetraspanin CD63, CD81 and CD9. A mouse IgG (MIgG) was used to capture non-exosomal particles. The captured exosomes were then triple-stained by fluorescent conjugated antibodies against the phenotypic marker of adipocyte (CD36) and macrophage (CD11b). Captured exosomes that were fluorescently positive for these proteins were counted and analyzed by ExoView analyzer. A fluorescent cutoff was set based on minimal detection of non-exosomal particles in MIgG capturing spots.

Exosome labeling and internalization by OC cells

Exosomes were labeled using an RNASelect Green Fluorescent staining kit (Thermo Fisher) to stain exosomal cargo RNA(63, 64). Briefly, collected exosomes were incubated with 500nM labeling solution for 20 minutes at 37°C. After that, the labeled exosomes were rinsed in PBS and re-concentrated by ultracentrifugation. $5x10^8$ /mL labeled exosomes were then added into growth media of OCSC1-F2 human OC cells and incubated for 2h. The internalization of labeled exosomes (GF-exosomes) in F2 cells was then analyzed by green fluorescent confocal microscopy.

Transwell Migration assay

1 × 10^5 OCSC1-F2 human OC cells were resuspended in serum-free Opti-MEM (Thermo Scientific) and seeded on trans-well inserts with a polyethylene terephthalate membrane pore size of 8.0 µm (Cat. No. 353097, Corning, NY). The inserts were placed on 24-well cell culture plates with RPIM1640 media with 10% FBS. After 24 h, inserts were washed three times with PBS, fixed with 4% paraformaldehyde, permeabilized with 0.01% Triton X-100 (Sigma-Aldrich, St. Louise, MO), and stained with crystal violet Sigma-Aldrich, St. Louise, MO). Migrated cells were viewed and counted using a phase-contrast microscope (ECHO Revolve microscope, San Diego, CA).

Luciferase reporter assay

The human 3'UTR of CBX7 gene encompassing the miR-421 binding site, and the 3'UTR of *CBX7* gene with point mutations were cloned into a pEZX-MT05 vector with Gluc/SeAP duo-Luciferase reporter. The dual luciferase reporter system (Secrete-Pair ™ Dual Luminescence Assay, GeneCopoeia, MD) allowed the normalization of luminescence to minimize variations in transfection efficiencies and cell viability. Each vector was transfected in OCSC1-F2 cells by lipofectamine (Invitrogen, Waltham, MA) at a concentration of 2 ug vector/10^6 cells. To assess the mRNA-miRNA interaction, each vector was co-transfected with miR-421 mimics (200pM/10^6 cells, Cat. No. 4464066, ThermoFisher Scientific, Waltham, MA). Twenty-four hours later, the cells were lysed and luciferase activity was detected using a multimode microplate reader (PerkinElmer/Fusion, Waltham, MA).

SDS-PAGE and Western blot analysis

Protein lysates were extracted from pelleted cells as previously described, and quantified using BCA assay (39, 89). Twenty micrograms of proteins were loaded in each well of 12%

polyacrylamide gel and PAGE and Western blots were performed, as previously described (39, 89).

RNA extraction and quantitative Reverse Transcriptase-Polymerase Chain Reaction (qRT-PCR) for CBX7

Total RNA was extracted from pelleted cells using RNeasy mini kit (Cat. No. 74106, Qiagen, Hilden, Germany). cDNA was obtained from 1 ug RNA using iScript cDNA synthesis kit (Bio-Rad, Hercules, CA). CBX7 and GAPDH qPCR was performed using SYBR Green Supermix (Bio-Rad, Hercules, CA) with 1:10 dilution of cDNA in a final volume of 10 µl according to manufacturer's instructions. The following primer sequences were used for CBX7 (Forward primer: 5'-CGAGTATCTGGTGAAGTGGAAA-3' and Reverse primer: 5'-GGGGGTCCAAGATGTGCT-3') and GAPDH (Forward primer: 5'-TGACGCTGGGGCTGGCATT-3' and Reverse primer: 5'-GGCTGGTGGTCCAGGGGT-3'). Primers were synthesized by Integrated DNA Technologies (San Diego, CA). qPCR was run on CFX96TM PCR detection system (Bio-Rad, Hercules, CA) using the following thermocycling parameters: 2 min 95°C; then 45 cycles of 20 s at 95°C and 1 min at 60°C. Control groups are incubated in growth media and experimental groups are incubated with ACM. No RT control was used as negative control. Relative expression was calculated using the comparative $\Delta\Delta$CT method with Control group as reference. All reactions were performed in triplicates.

RNA extraction and quantitative PCR for miR-421

Total RNA was extracted from ACM-derived exosomes using miRNeasy mini kit (Cat. No. 74106, Qiagen, Hilden, Germany). To determine miR-421 levels in exosomes, qPCR was performed with TaqMan miRNA assay kit (ThermoFisher Scientific, Waltham, MA). Briefly, miRNAs were reverse transcribed with the miRNA Reverse Transcription reagent and amplified with Taqman PCR

reagents, which were specifically designed for detecting mature miR-421 sequence (AUCAACAGACAUUAAUUGGGCGC). U6 snRNA (mature sequence: GTGCTCGCTTCGGCAGCACATATACTAAAATTGGAACGATACAGAGAAGATTAGCATGGCC CCTGCGCAAGGATGACACGCAAATTCGTGAAGCGTTCCATATTTT) was used as the internal control. Relative expression was calculated by 2−ΔΔCt method according to published protocol (90).

Statistical Analysis

Data were graphed and analyzed using Prism 9 (RRID:SCR_002798; GraphPad Software, Inc, Boston, MA). Unpaired t test or One-way ANOVA were used and p values <0.05 were considered statistically significant.

Declarations

Ethics approval and consent to participate

Sample collection was obtained with informed consent with prior approval from Karmanos Cancer Center and the University of South Florida IRB.

Consent for publication

Not applicable.

Availability of data and materials

Not applicable.

Competing interests

The authors declare no potential conflicts of interest.

Funding

This work is supported in part by NIH R01 CA199004 to GM and the Janet Burros Memorial Foundation.

Authors' contributions

YZ – Conceptualization, Investigation, Methodology

RT – Investigation, Validation, Visualization

MM – Investigation

TW – Investigation

AF – Investigation

HC – Investigation

452 MG – Investigation

453 NA – Formal analysis

454 RG – Resources

455 MA – Resources

456 TR – Resources

457 ZZ – Conceptualization

458 MC – Conceptualization, Writing – review and editing

459 GM – Conceptualization, Funding acquisition, Writing – review and editing

460 AA – Conceptualization, Project administration, Investigation, Writing – original draft

Table 1. Patient characteristics.

Patient number	Age	Menopausal stage	Diagnosis
652	64	Postmenopausal	Grade 3 endometrial cancer
654	50	Premenopausal	Uterine leiomyoma
620	68	Postmenopausal	Ovarian cyst
626	33	Premenopausal	Cervical cancer
628	40	Premenopausal	Uterine leiomyoma
568	52	Premenopausal	Endometrial hyperplasia

Table 2. List of miRNAs predicted by mirTarBase to target CBX7

hsa-miR-421
hsa-miR-125b-5p
has-miR-181b-5p
has-miR-766-3p
hsa-miR-6818-3p
hsa-miR-4515
hsa-miR-6077
hsa-miR-7-5p
hsa-miR-3169
hsa-miR-4700-3p
hsa-miR-548ay-3p
hsa-miR-548at-3p
hsa-miR-548as-3p
hsa-miR-548t-3p
hsa-miR-548ap-3p
hsa-miR-548aa
hsa-miR-19b-3p
hsa-miR-19a-3p
hsa-miR-18a-3p

Table 3. List of miRNAs predicted by TargetScanHuman to target CBX7 (45 out of 918 are listed)

hsa-miR-224-5p
hsa-miR-125b-5p
hsa-miR-4319
hsa-miR-125a-5p
hsa-miR-874-3p
hsa-miR-9-5p
hsa-miR-219a-2-3p
hsa-miR-331-3p
hsa-miR-193a-3p
hsa-miR-193b-3p
hsa-miR-181b-5p
hsa-miR-181c-5p
hsa-miR-181d-5p
hsa-miR-181a-5p
hsa-miR-4262
hsa-miR-182-5p
hsa-miR-218-5p
hsa-miR-19b-3p
hsa-miR-19a-3p
hsa-miR-181d-5p
hsa-miR-181a-5p
hsa-miR-181c-5p
hsa-miR-181b-5p

hsa-miR-4262

hsa-miR-129-5p

hsa-miR-3653-3p

hsa-miR-3658

hsa-miR-570-3p

hsa-miR-1260b

hsa-miR-1260a

hsa-miR-1224-3p

hsa-miR-4433a-5p

hsa-miR-5588-3p

hsa-miR-6128

hsa-miR-875-3p

has-miR-421

hsa-miR-1299

hsa-miR-518c-5p

hsa-miR-6824-3p

hsa-miR-3191-5p

hsa-miR-6764-3p

hsa-miR-326

hsa-miR-330-5p

hsa-miR-3675-3p

Figures and Figures Legends

Figure 1. Adipose conditioned media (ACM) downregulate CBX7 and enhance migratory capacity in ovarian cancer cells. A panel of human ovarian cancer cells were cultured for 5 days in ACM from omental explants isolated from a female patient with a benign gynecological condition. No treatment control cells (NT) were cultured in growth media. **(A)** Levels of CBX7 were determined by Western blot analysis; **(B)** Representative microscopic images show acquisition of a fibroblastic spindle-like morphology; **(C)** Western blot analysis for EMT markers in OCSC1-F2 human ovarian cancer cells; **(D)** *top panel*, OCSC1-F2 human ovarian cancer cells were cultured in ACM or growth media for 5 days, trypsinized, washed, and placed in trans-well inserts with growth media. Note enhanced migration in cells previously cultured with ACM; *bottom panel*, quantification of migration (n=8); *** $p < 0.0001$. Data are presented as mean +/- SEM. Unpaired t-test was used to determine statistical significance.

552 **Figure 2. Characterization of exosomes derived from adipose conditioned media (ACM)**.
553 Exosomes were isolated from ACM by differential ultracentrifugation. **(A)** Representative particle
554 size distribution (ave = 137 nm) of ACM-derived exosomes analyzed by Nanoparticle Tracking
555 Analysis; **(B)** Representative transmission electron microscopy image showing the doughnut-
556 shaped morphology of the isolated exosomes; **(C)** Representative Western blot analysis of ACM-
557 derived exosomes showing expression of exosomal markers CD63 and CD9 and absence of the
558 endoplasmic reticulum marker, calnexin; Protein lysate of Adipose-Derived Mesenchymal Stem
559 Cells (ADMSC) is used as positive control of calnexin. **(D)** Representative images from ExoView
560 analysis showing majority of captured exosomes are positive for the adipocyte marker, CD36,
561 and negative for the macrophage marker, CD11b; **(E)** Quantification of D and showing data from
562 6 individual patients. Data are presented as mean +/- SEM (n=6). Unpaired t-test was used to
563 determine statistical significance. Data shown are for exosomes 654 and 652. Similar results were
564 observed with other exosomal preparations.
565
566

Figure 3. Adipose-derived exosomes are internalized by human ovarian cancer cells via endocytosis and induce down-regulation of CBX7. **(A)** Labelled ACM-derived exosomes were internalized by mCherry-labelled OCSC1-F2 cells; **(B)** Human R182 ovarian cancer cells were treated for 48h with adipose-derived exosomes ($5x10^8$ exosomes/ml) isolated from patients in Table 1. *top panel*, levels of CBX7 determined by Western blot analysis. * denotes preparations able to down-regulate CBX7. *bottom panel*, densitometry quantification of top panel; **(C)** OCSC1-F2 human ovarian cancer cells were treated with ACM, exosomes (exo), exosome-depleted ACM (ACM-exo) or exosome with Nystatin and levels of CBX7 determined by Western blot analysis; **(D)** OVCAR3 human ovarian cancer cells were treated with ACM, exosomes (exo), or exosome-depleted ACM (ACM-exo) and levels of CBX7 determined by Western blot analysis.

Figure 4. Adipose-derived exosomal miR-421 targets CBX7. (A) Venn diagram analysis from predicted miRNAs targeting CBX7 from mirTarBase (Table 2) and TargetScanHuman (Table 3) and lists of adipocyte specific miRNA from *Adicer* KO mice and patients with congenital lipodystrophy (CGL) (65) shows miR-421 as the only common element in the overlap; **(B)** OCSC1-F2 human ovarian cancer cells were treated with adipose-derived exosomes (exo) in the presence of anti-miR-421 or anti-miR negative control (-ve con Anti-mir) and effect on CBX7 was determined by Western blot analysis; NT, no treatment control **(C)** OCSC1-F2 human ovarian cancer cells were treated with miR-421 mimic and the effect on CBX7 was determined by Western blot analysis; Neg, non-specific miRNA; **(D)** plasmid design for luciferase reporter system carrying CBX7 3' UTR predicted to be the binding site for miR-421 (pCBX7) and its mutated version (pCBX7mut). Sequence of human miR-421 (hsa-mir-421) is also shown; **(E)** Luciferase reporters were transfected in OCSC1-F2 human OC cells in the presence or absence of miR-421 or non-specific miRNA (Neg) as indicated, and levels of luciferase were measured as surrogate of binding affinity; **(F)** miR-421 was quantified in adipose- derived exosomes using qPCR. Note that exosomes successful in downregulating CBX7 (columns with red data points) contain higher levels of mir-421. Data are presented as mean +/- SEM (n=3). Ordinary One way ANOVA with Tukey's multiple comparison test was used to determine statistical significance.

Supplementary Figure 1. Loss of CBX7 is sufficient to enhance migration. (A) CBX7 was stably knocked-down in OCSC1-F2 human OC cells using CRISPR-Cas9. **(A)** Expression of CBX7 was determined by Western blot analysis; **(B)** Effect on migration was determined using trans-well migration assay. WT, wild-type; g1, guide RNA 1; g2, guide RNA 2.

Supplementary Figure 2. CBX7 protein downregulation is not associated with changes in mRNA. OVCAR3 and OCSC1-F1 human OC cells were cultured in ACM for 5 days and effect on CBX7 mRNA was determined by qPCR. NT, Control no treatment cells were cultured in growth media.

References

1. Jin MZ, Jin WL. The updated landscape of tumor microenvironment and drug repurposing. Signal Transduct Target Ther. 2020;5(1):166.
2. Farc O, Cristea V. An overview of the tumor microenvironment, from cells to complex networks (Review). Exp Ther Med. 2021;21(1):96.
3. Mbeunkui F, Johann DJ, Jr. Cancer and the tumor microenvironment: a review of an essential relationship. Cancer Chemother Pharmacol. 2009;63(4):571-82.
4. Yao H, He S. Multifaceted role of cancerassociated adipocytes in the tumor microenvironment (Review). Mol Med Rep. 2021;24(6).
5. Dumas JF, Brisson L. Interaction between adipose tissue and cancer cells: role for cancer progression. Cancer Metastasis Rev. 2021;40(1):31-46.
6. Laurent V, Toulet A, Attane C, Milhas D, Dauvillier S, Zaidi F, et al. Periprostatic Adipose Tissue Favors Prostate Cancer Cell Invasion in an Obesity-Dependent Manner: Role of Oxidative Stress. Mol Cancer Res. 2019;17(3):821-35.
7. Wu Q, Li B, Li Z, Li J, Sun S, Sun S. Cancer-associated adipocytes: key players in breast cancer progression. J Hematol Oncol. 2019;12(1):95.
8. Xiong X, Wen YA, Fairchild R, Zaytseva YY, Weiss HL, Evers BM, et al. Upregulation of CPT1A is essential for the tumor-promoting effect of adipocytes in colon cancer. Cell Death Dis. 2020;11(9):736.
9. Nieman KM, Kenny HA, Penicka CV, Ladanyi A, Buell-Gutbrod R, Zillhardt MR, et al. Adipocytes promote ovarian cancer metastasis and provide energy for rapid tumor growth. Nat Med. 2011;17(11):1498-503.
10. Cardenas C, Montagna MK, Pitruzzello M, Lima E, Mor G, Alvero AB. Adipocyte microenvironment promotes Bclxl expression and confers chemoresistance in ovarian cancer cells. Apoptosis. 2017;22(4):558-69.
11. Torre LA, Trabert B, DeSantis CE, Miller KD, Samimi G, Runowicz CD, et al. Ovarian cancer statistics, 2018. CA Cancer J Clin. 2018;68(4):284-96.
12. Cardenas C, Alvero AB, Yun BS, Mor G. Redefining the origin and evolution of ovarian cancer: a hormonal connection. Endocr Relat Cancer. 2016;23(9):R411-22.
13. Bowtell DD, Bohm S, Ahmed AA, Aspuria PJ, Bast RC, Jr., Beral V, et al. Rethinking ovarian cancer II: reducing mortality from high-grade serous ovarian cancer. Nat Rev Cancer. 2015;15(11):668-79.
14. Nezhat FR, Pejovic T, Finger TN, Khalil SS. Role of minimally invasive surgery in ovarian cancer. J Minim Invasive Gynecol. 2013;20(6):754-65.
15. Park J, Morley TS, Kim M, Clegg DJ, Scherer PE. Obesity and cancer--mechanisms underlying tumour progression and recurrence. Nat Rev Endocrinol. 2014;10(8):455-65.
16. Thrall MM, Goff BA, Symons RG, Flum DR, Gray HJ. Thirty-day mortality after primary cytoreductive surgery for advanced ovarian cancer in the elderly. Obstet Gynecol. 2011;118(3):537-47.

17. Hamilton CA, Miller A, Miller C, Krivak TC, Farley JH, Chernofsky MR, et al. The impact of disease distribution on survival in patients with stage III epithelial ovarian cancer cytoreduced to microscopic residual: A gynecologic oncology group study. Gynecol Oncol. 2011.
18. Bhusari PA, Khairnar KB. Greater Omental Pancake Tumour due to Metastasis of Ovarian Cancer - A Cadaveric Study. J Clin Diagn Res. 2014;8(1):142-3.
19. Naora H, Montell DJ. Ovarian cancer metastasis: integrating insights from disparate model organisms. Nat Rev Cancer. 2005;5(5):355-66.
20. Ladanyi A, Mukherjee A, Kenny HA, Johnson A, Mitra AK, Sundaresan S, et al. Adipocyte-induced CD36 expression drives ovarian cancer progression and metastasis. Oncogene. 2018;37(17):2285-301.
21. Lengyel E, Litchfield LM, Mitra AK, Nieman KM, Mukherjee A, Zhang Y, et al. Metformin inhibits ovarian cancer growth and increases sensitivity to paclitaxel in mouse models. Am J Obstet Gynecol. 2015;212(4):479.e1-.e10.
22. Nieman KM, Romero IL, Van Houten B, Lengyel E. Adipose tissue and adipocytes support tumorigenesis and metastasis. Biochim Biophys Acta. 2013;1831(10):1533-41.
23. Yang J, Zaman MM, Vlasakov I, Roy R, Huang L, Martin CR, et al. Adipocytes promote ovarian cancer chemoresistance. Sci Rep. 2019;9(1):13316.
24. Cardenas C, Montagna MK, Pitruzzello M, Lima E, Mor G, Alvero AB. Adipocyte microenvironment promotes Bcl(xl) expression and confers chemoresistance in ovarian cancer cells. Apoptosis. 2017;22(4):558-69.
25. Ku M, Koche RP, Rheinbay E, Mendenhall EM, Endoh M, Mikkelsen TS, et al. Genomewide analysis of PRC1 and PRC2 occupancy identifies two classes of bivalent domains. PLoS Genet. 2008;4(10):e1000242.
26. Scott CL, Gil J, Hernando E, Teruya-Feldstein J, Narita M, Martinez D, et al. Role of the chromobox protein CBX7 in lymphomagenesis. Proc Natl Acad Sci U S A. 2007;104(13):5389-94.
27. Kotake Y, Cao R, Viatour P, Sage J, Zhang Y, Xiong Y. pRB family proteins are required for H3K27 trimethylation and Polycomb repression complexes binding to and silencing p16INK4alpha tumor suppressor gene. Genes & development. 2007;21(1):49-54.
28. Dietrich N, Bracken AP, Trinh E, Schjerling CK, Koseki H, Rappsilber J, et al. Bypass of senescence by the polycomb group protein CBX8 through direct binding to the INK4A-ARF locus. The EMBO Journal. 2007;26(6):1637-48.
29. Tolhuis B, de Wit E, Muijrers I, Teunissen H, Talhout W, van Steensel B, et al. Genome-wide profiling of PRC1 and PRC2 Polycomb chromatin binding in Drosophila melanogaster. Nature genetics. 2006;38(6):694-9.
30. Zhu X, Qin M, Li C, Zeng W, Bei C, Tan C, et al. Downregulated Expression of Chromobox Homolog 7 in Hepatocellular Carcinoma. Genet Test Mol Biomarkers. 2019;23(5):348-52.
31. Tan C, Bei C, Zhu X, Zhang Y, Qin L, Tan S. Single Nucleotide Polymorphisms of CBX4 and CBX7 Decrease the Risk of Hepatocellular Carcinoma. Biomed Res Int. 2019;2019:6436825.
32. Federico A, Sepe R, Cozzolino F, Piccolo C, Iannone C, Iacobucci I, et al. The complex CBX7-PRMT1 has a critical role in regulating E-cadherin gene expression and cell migration. Biochim Biophys Acta Gene Regul Mech. 2019;1862(4):509-21.
33. Yongyu Z, Lewei Y, Jian L, Yuqin S. MicroRNA-18a targets IRF2 and CBX7 to promote cell proliferation in hepatocellular carcinoma. Oncol Res. 2018.

34. Gil J, Bernard D, Martínez D, Beach D. Polycomb CBX7 has a unifying role in cellular lifespan. Nat Cell Biol. 2004;6(1):67-72.
35. Bao Z, Xu X, Liu Y, Chao H, Lin C, Li Z, et al. CBX7 negatively regulates migration and invasion in glioma via Wnt/beta-catenin pathway inactivation. Oncotarget. 2017;8(24):39048-63.
36. Sepe R, Formisano U, Federico A, Forzati F, Bastos AU, D'Angelo D, et al. CBX7 and HMGA1b proteins act in opposite way on the regulation of the SPP1 gene expression. Oncotarget. 2015;6(5):2680-92.
37. Pallante P, Forzati F, Federico A, Arra C, Fusco A. Polycomb protein family member CBX7 plays a critical role in cancer progression. Am J Cancer Res. 2015;5(5):1594-601.
38. Cacciola NA, Sepe R, Forzati F, Federico A, Pellecchia S, Malapelle U, et al. Restoration of CBX7 expression increases the susceptibility of human lung carcinoma cells to irinotecan treatment. Naunyn Schmiedebergs Arch Pharmacol. 2015;388(11):1179-86.
39. Li J, Alvero AB, Nuti S, Tedja R, Roberts CM, Pitruzzello M, et al. CBX7 binds the E-box to inhibit TWIST-1 function and inhibit tumorigenicity and metastatic potential. Oncogene. 2020;39(20):3965-79.
40. Tkach M, Thery C. Communication by Extracellular Vesicles: Where We Are and Where We Need to Go. Cell. 2016;164(6):1226-32.
41. Zhang ZG, Buller B, Chopp M. Exosomes - beyond stem cells for restorative therapy in stroke and neurological injury. Nat Rev Neurol. 2019;15(4):193-203.
42. Mathieu M, Martin-Jaular L, Lavieu G, Thery C. Specificities of secretion and uptake of exosomes and other extracellular vesicles for cell-to-cell communication. Nat Cell Biol. 2019;21(1):9-17.
43. Dai J, Su Y, Zhong S, Cong L, Liu B, Yang J, et al. Exosomes: key players in cancer and potential therapeutic strategy. Signal Transduct Target Ther. 2020;5(1):145.
44. Lan J, Sun L, Xu F, Liu L, Hu F, Song D, et al. M2 Macrophage-Derived Exosomes Promote Cell Migration and Invasion in Colon Cancer. Cancer Res. 2019;79(1):146-58.
45. Okoye IS, Coomes SM, Pelly VS, Czieso S, Papayannopoulos V, Tolmachova T, et al. MicroRNA-containing T-regulatory-cell-derived exosomes suppress pathogenic T helper 1 cells. Immunity. 2014;41(1):89-103.
46. Zhao H, Yang L, Baddour J, Achreja A, Bernard V, Moss T, et al. Tumor microenvironment derived exosomes pleiotropically modulate cancer cell metabolism. Elife. 2016;5:e10250.
47. Jiang C, Zhang N, Hu X, Wang H. Tumor-associated exosomes promote lung cancer metastasis through multiple mechanisms. Molecular Cancer. 2021;20(1):117.
48. Tian W, Liu S, Li B. Potential Role of Exosomes in Cancer Metastasis. Biomed Res Int. 2019;2019:4649705.
49. Guo Y, Ji X, Liu J, Fan D, Zhou Q, Chen C, et al. Effects of exosomes on pre-metastatic niche formation in tumors. Molecular Cancer. 2019;18(1):39.
50. O'Brien J, Hayder H, Zayed Y, Peng C. Overview of MicroRNA Biogenesis, Mechanisms of Actions, and Circulation. Front Endocrinol (Lausanne). 2018;9:402.
51. Saliminejad K, Khorram Khorshid HR, Soleymani Fard S, Ghaffari SH. An overview of microRNAs: Biology, functions, therapeutics, and analysis methods. J Cell Physiol. 2019;234(5):5451-65.
52. Mohr AM, Mott JL. Overview of microRNA biology. Semin Liver Dis. 2015;35(1):3-11.

737 53. Hill M, Tran N. miRNA interplay: mechanisms and consequences in cancer. Dis Model
738 Mech. 2021;14(4).
739 54. Bushati N, Cohen SM. microRNA functions. Annu Rev Cell Dev Biol. 2007;23:175-205.
740 55. Bhome R, Del Vecchio F, Lee GH, Bullock MD, Primrose JN, Sayan AE, et al. Exosomal
741 microRNAs (exomiRs): Small molecules with a big role in cancer. Cancer Lett. 2018;420:228-35.
742 56. Cheng L, Sharples RA, Scicluna BJ, Hill AF. Exosomes provide a protective and enriched
743 source of miRNA for biomarker profiling compared to intracellular and cell-free blood. J
744 Extracell Vesicles. 2014;3.
745 57. Villarroya-Beltri C, Gutierrez-Vazquez C, Sanchez-Cabo F, Perez-Hernandez D, Vazquez J,
746 Martin-Cofreces N, et al. Sumoylated hnRNPA2B1 controls the sorting of miRNAs into exosomes
747 through binding to specific motifs. Nat Commun. 2013;4:2980.
748 58. Thery C, Witwer KW, Aikawa E, Alcaraz MJ, Anderson JD, Andriantsitohaina R, et al.
749 Minimal information for studies of extracellular vesicles 2018 (MISEV2018): a position
750 statement of the International Society for Extracellular Vesicles and update of the MISEV2014
751 guidelines. J Extracell Vesicles. 2018;7(1):1535750.
752 59. Di Nicola V. Omentum a powerful biological source in regenerative surgery. Regen Ther.
753 2019;11:182-91.
754 60. Wu D, Yan J, Shen X, Sun Y, Thulin M, Cai Y, et al. Profiling surface proteins on individual
755 exosomes using a proximity barcoding assay. Nature communications. 2019;10(1):3854.
756 61. Larssen P, Wik L, Czarnewski P, Eldh M, Löf L, Ronquist KG, et al. Tracing Cellular Origin
757 of Human Exosomes Using Multiplex Proximity Extension Assays. Mol Cell Proteomics.
758 2017;16(3):502-11.
759 62. Castillo J, Bernard V, San Lucas FA, Allenson K, Capello M, Kim DU, et al. Surfaceome
760 profiling enables isolation of cancer-specific exosomal cargo in liquid biopsies from pancreatic
761 cancer patients. Ann Oncol. 2018;29(1):223-9.
762 63. Zhang Y, Li C, Qin Y, Cepparulo P, Millman M, Chopp M, et al. Small extracellular vesicles
763 ameliorate peripheral neuropathy and enhance chemotherapy of oxaliplatin on ovarian cancer.
764 J Extracell Vesicles. 2021;10(5):e12073.
765 64. Li M, Zeringer E, Barta T, Schageman J, Cheng A, Vlassov AV. Analysis of the RNA content
766 of the exosomes derived from blood serum and urine and its potential as biomarkers. Philos
767 Trans R Soc Lond B Biol Sci. 2014;369(1652).
768 65. Thomou T, Mori MA, Dreyfuss JM, Konishi M, Sakaguchi M, Wolfrum C, et al. Adipose-
769 derived circulating miRNAs regulate gene expression in other tissues. Nature.
770 2017;542(7642):450-5.
771 66. Nieman KM, Kenny HA, Penicka CV, Ladanyi A, Buell-Gutbrod R, Zillhardt MR, et al.
772 Adipocytes promote ovarian cancer metastasis and provide energy for rapid tumor growth.
773 Nature Medicine. 2011;17(11):1498-503.
774 67. Mukherjee A, Chiang CY, Daifotis HA, Nieman KM, Fahrmann JF, Lastra RR, et al.
775 Adipocyte-Induced FABP4 Expression in Ovarian Cancer Cells Promotes Metastasis and
776 Mediates Carboplatin Resistance. Cancer Res. 2020;80(8):1748-61.
777 68. Zhang J, Li S, Li L, Li M, Guo C, Yao J, et al. Exosome and exosomal microRNA: trafficking,
778 sorting, and function. Genomics Proteomics Bioinformatics. 2015;13(1):17-24.
779 69. Luo X, Jean-Toussaint R, Sacan A, Ajit SK. Differential RNA packaging into small
780 extracellular vesicles by neurons and astrocytes. Cell Commun Signal. 2021;19(1):75.

781 70. Huang Q, Yang J, Zheng J, Hsueh C, Guo Y, Zhou L. Characterization of selective exosomal
782 microRNA expression profile derived from laryngeal squamous cell carcinoma detected by next
783 generation sequencing. Oncol Rep. 2018;40(5):2584-94.
784 71. Garcia-Martin R, Wang G, Brandao BB, Zanotto TM, Shah S, Kumar Patel S, et al.
785 MicroRNA sequence codes for small extracellular vesicle release and cellular retention. Nature.
786 2022;601(7893):446-51.
787 72. Kalra H, Drummen GP, Mathivanan S. Focus on Extracellular Vesicles: Introducing the
788 Next Small Big Thing. Int J Mol Sci. 2016;17(2):170.
789 73. Zhang M, Xie X, Lee AH, Binns CW, Holman CD. Body mass index in relation to ovarian
790 cancer survival. Cancer Epidemiol Biomarkers Prev. 2005;14(5):1307-10.
791 74. Akhavan S, Ghahghaei-Nezamabadi A, Modaresgilani M, Mousavi AS, Sepidarkish M,
792 Tehranian A, et al. Impact of diabetes mellitus on epithelial ovarian cancer survival. BMC
793 cancer. 2018;18(1):1246.
794 75. Qiu W, Lu H, Qi Y, Wang X. Dietary fat intake and ovarian cancer risk: a meta-analysis of
795 epidemiological studies. Oncotarget. 2016;7(24):37390-406.
796 76. Kangas R, Tormakangas T, Fey V, Pursiheimo J, Miinalainen I, Alen M, et al. Aging and
797 serum exomiR content in women-effects of estrogenic hormone replacement therapy. Sci Rep.
798 2017;7:42702.
799 77. Shao JL, Li H, Zhang XR, Zhang X, Li ZZ, Jiao GL, et al. Identification of Serum Exosomal
800 MicroRNA Expression Profiling in Menopausal Females with Osteoporosis by High-throughput
801 Sequencing. Curr Med Sci. 2020;40(6):1161-9.
802 78. Kangas R, Morsiani C, Pizza G, Lanzarini C, Aukee P, Kaprio J, et al. Menopause and
803 adipose tissue: miR-19a-3p is sensitive to hormonal replacement. Oncotarget. 2018;9(2):2279-
804 94.
805 79. Ghoshal B, Bertrand E, Bhattacharyya SN. Non-canonical argonaute loading of
806 extracellular vesicle-derived exogenous single-stranded miRNA in recipient cells. J Cell Sci.
807 2021;134(9).
808 80. Horie K, Nanashima N, Yokoyama Y, Yoshioka H, Watanabe J. Exosomal MicroRNA as
809 Biomarkers for Diagnosing or Monitoring the Progression of Ovarian Clear Cell Carcinoma: A
810 Pilot Study. Molecules. 2022;27(12).
811 81. Shiao MS, Chang JM, Lertkhachonsuk AA, Rermluk N, Jinawath N. Circulating Exosomal
812 miRNAs as Biomarkers in Epithelial Ovarian Cancer. Biomedicines. 2021;9(10).
813 82. Alvero AB, Kim D, Lima E, Sumi NJ, Lee JS, Cardenas C, et al. Novel approach for the
814 detection of intraperitoneal micrometastasis using an ovarian cancer mouse model. Sci Rep.
815 2017;7:40989.
816 83. Craveiro V, Yang-Hartwich Y, Holmberg JC, Sumi NJ, Pizzonia J, Griffin B, et al.
817 Phenotypic modifications in ovarian cancer stem cells following Paclitaxel treatment. Cancer
818 Med. 2013;2(6):751-62.
819 84. Kelly MG, Alvero AB, Chen R, Silasi DA, Abrahams VM, Chan S, et al. TLR-4 signaling
820 promotes tumor growth and paclitaxel chemoresistance in ovarian cancer. Cancer Res.
821 2006;66(7):3859-68.
822 85. Tedja R, Alvero AB, Fox A, Cardenas C, Pitruzzello M, Chehade H, et al. Generation of
823 Stable Epithelial-Mesenchymal Hybrid Cancer Cells with Tumorigenic Potential. Cancers.
824 2023;15(3).

825 86. Zhang Y, Qin Y, Chopp M, Li C, Kemper A, Liu X, et al. Ischemic Cerebral Endothelial Cell-
826 Derived Exosomes Promote Axonal Growth. Stroke. 2020;51(12):3701-12.
827 87. Zhang Y, Chopp M, Liu XS, Katakowski M, Wang X, Tian X, et al. Exosomes Derived from
828 Mesenchymal Stromal Cells Promote Axonal Growth of Cortical Neurons. Mol Neurobiol.
829 2017;54(4):2659-73.
830 88. Théry C, Witwer KW, Aikawa E, Alcaraz MJ, Anderson JD, Andriantsitohaina R, et al.
831 Minimal information for studies of extracellular vesicles 2018 (MISEV2018): a position
832 statement of the International Society for Extracellular Vesicles and update of the MISEV2014
833 guidelines. Journal of Extracellular Vesicles. 2018;7(1):1535750.
834 89. Tedja R, Roberts CM, Alvero AB, Cardenas C, Yang-Hartwich Y, Spadinger S, et al. Protein
835 kinase Cα-mediated phosphorylation of Twist1 at Ser-144 prevents Twist1 ubiquitination and
836 stabilizes it. J Biol Chem. 2019;294(13):5082-93.
837 90. Livak KJ, Schmittgen TD. Analysis of relative gene expression data using real-time
838 quantitative PCR and the 2(-Delta Delta C(T)) Method. Methods. 2001;25(4):402-8.
839

840

Figure 1

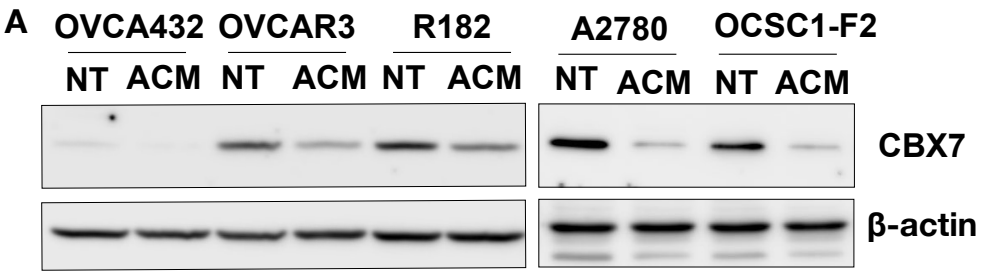
A
OVCA432
OVCAR3
R182
A2780
OCSC1-F2
NT ACM NT ACM NT ACM NT ACM NT ACM
CBX7
β-actin

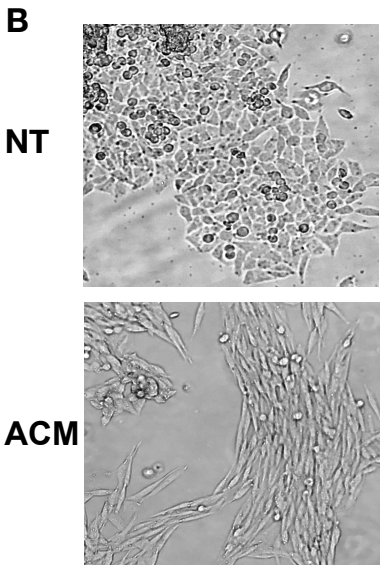
B
NT
ACM

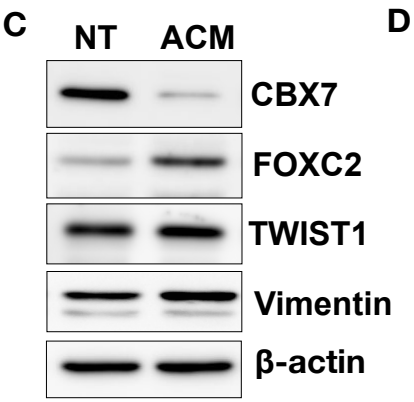
C
NT ACM
CBX7
FOXC2
TWIST1
Vimentin
β-actin

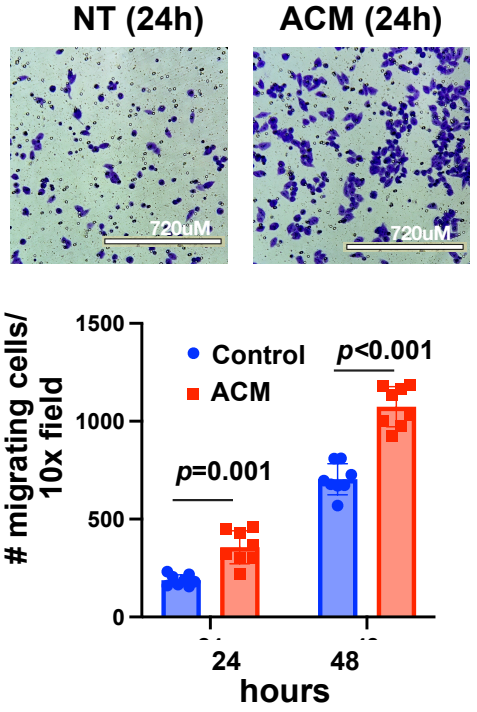
D
NT (24h)
ACM (24h)
720uM
720uM
migrating cells/ 10x field
1500
1000
500
0
Control
ACM
p<0.001
p=0.001
24
48
hours

Figure 2. USE NEW TIFF from Yi

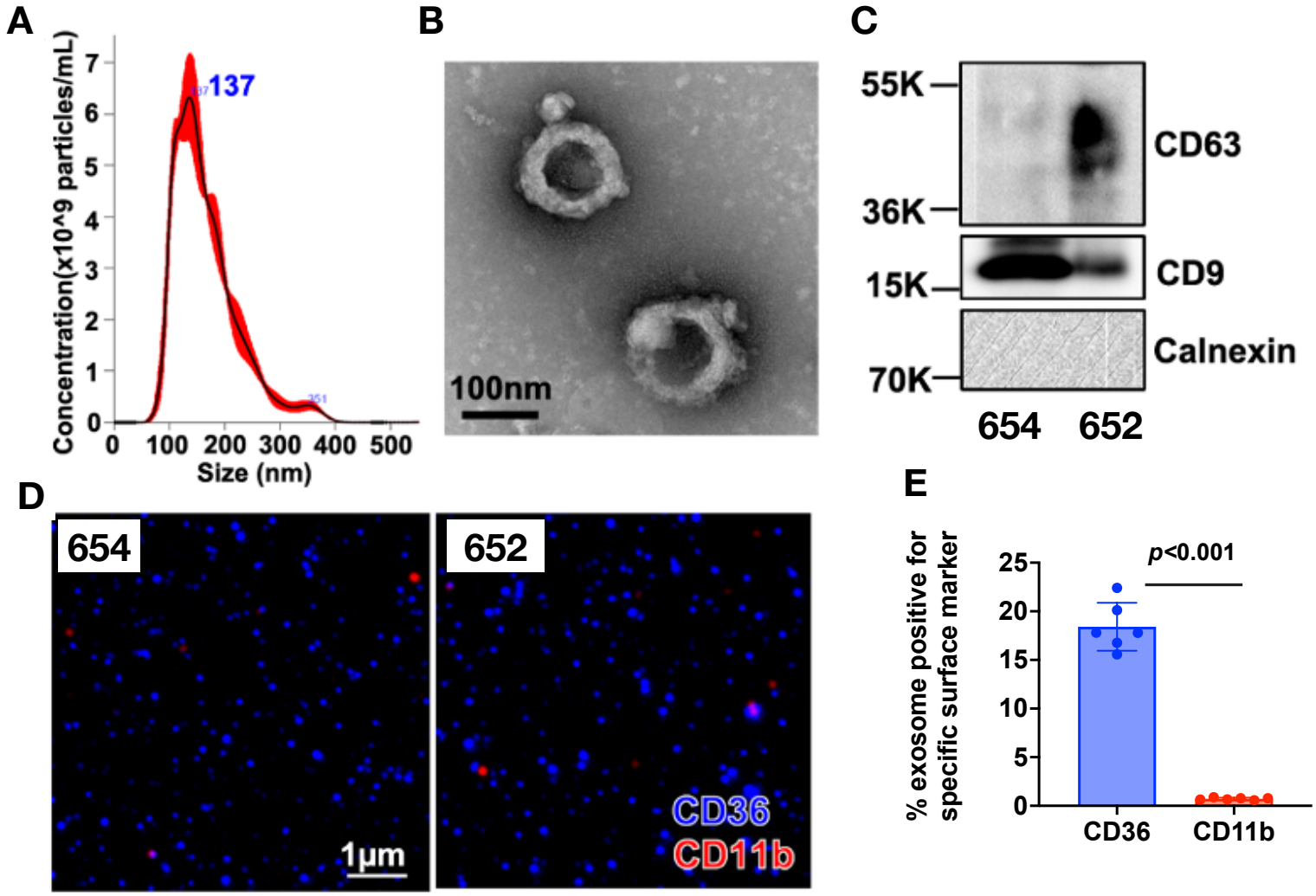

Figure 3

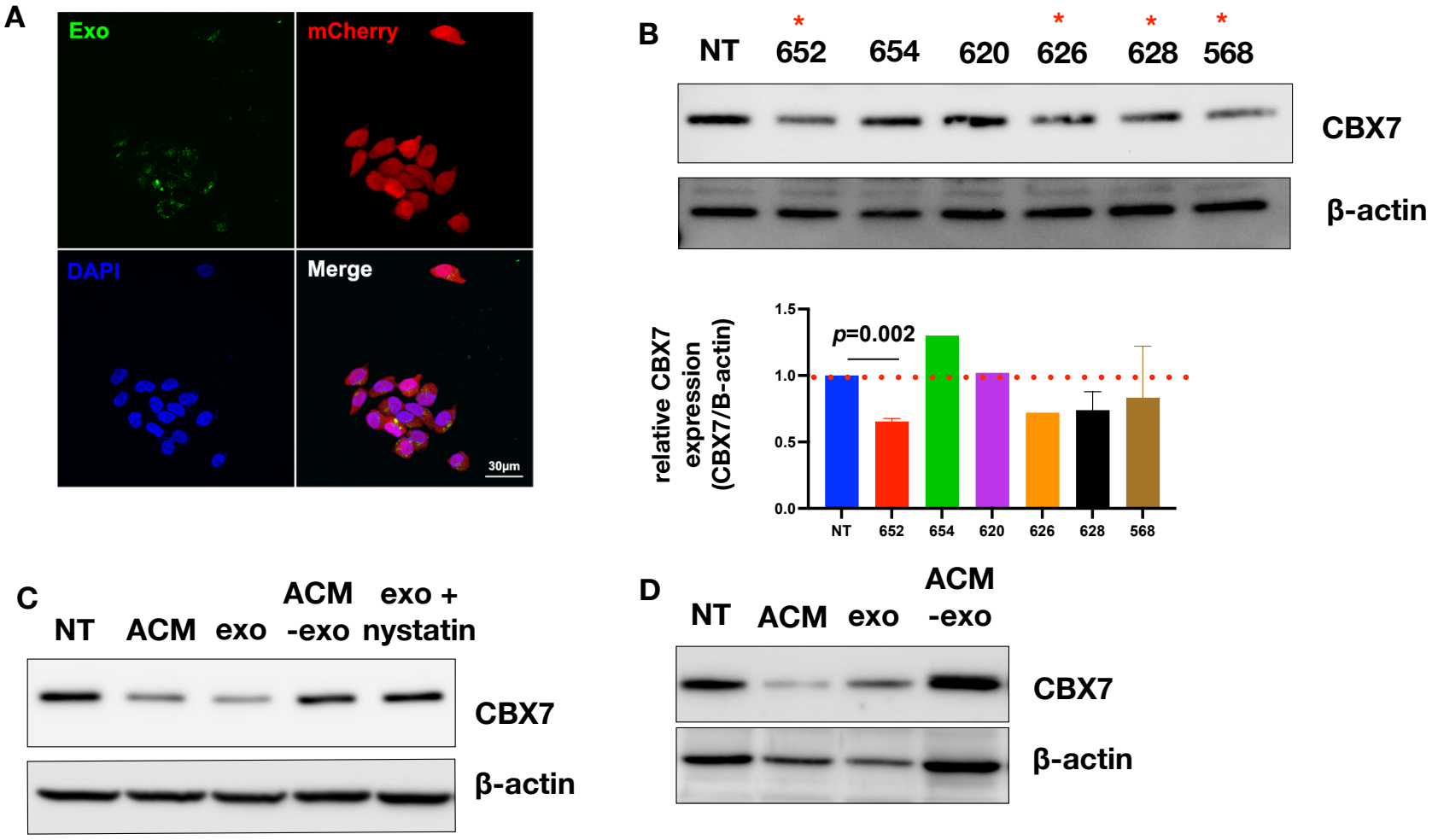
A
Exo
mCherry
DAPI
Merge
30μm
B
NT
652
654
620
626
628
568
CBX7
β-actin
relative CBX7 expression (CBX7/B-actin)
p=0.002
1.5
1.0
0.5
0.0
C
NT
ACM
exo
ACM -exo
exo + nystatin
CBX7
β-actin
D
NT
ACM
exo
ACM -exo
CBX7
β-actin

Figure 4

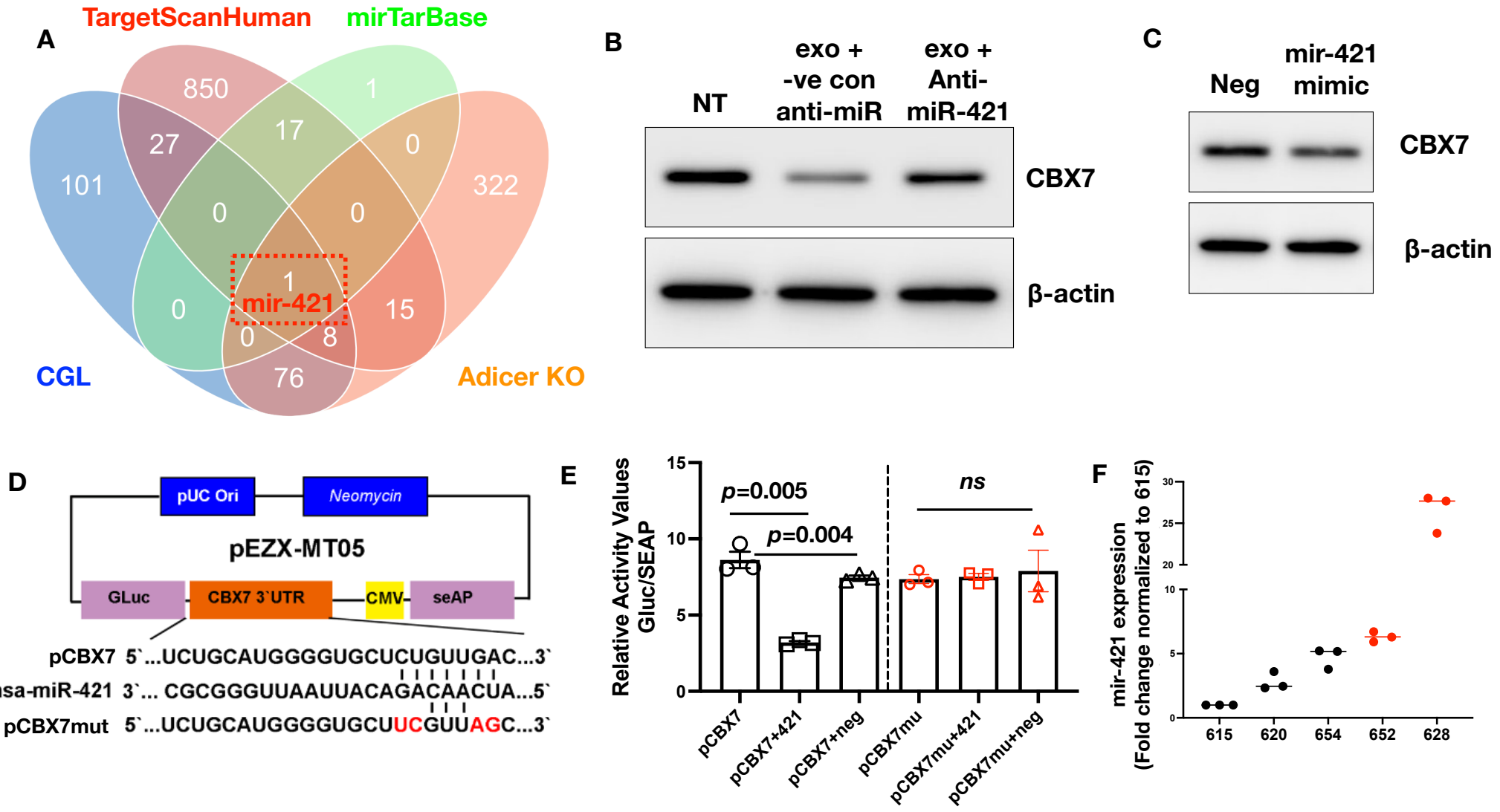
A
TargetScanHuman
mirTarBase
850
1
27
17
0
101
322
0
0
1
mir-421
0
15
0
8
76
CGL
Adicer KO
B
NT
exo +
-ve con
anti-miR
exo +
Anti-
miR-421
CBX7
β-actin
C
Neg
mir-421
mimic
CBX7
β-actin
D
pUC Ori
Neomycin
pEZX-MT05
GLuc
CBX7 3`UTR
CMV
seAP
pCBX7 5`...UCUGCAUGGGGUGCUCUGUUGAC...3`
hsa-miR-421 3`... CGCGGGUUAAUUACAGACAACUA...5`
pCBX7mut 5`...UCUGCAUGGGGUGCUUCGUUAGC...3`
E
Relative Activity Values
Gluc/SEAP
p=0.005
p=0.004
ns
pCBX7
pCBX7+421
pCBX7+neg
pCBX7mu
pCBX7mu+421
pCBX7mu+neg
F
mir-421 expression
(Fold change normalized to 615)
615
620
654
652
628

Supplementary Figure 1

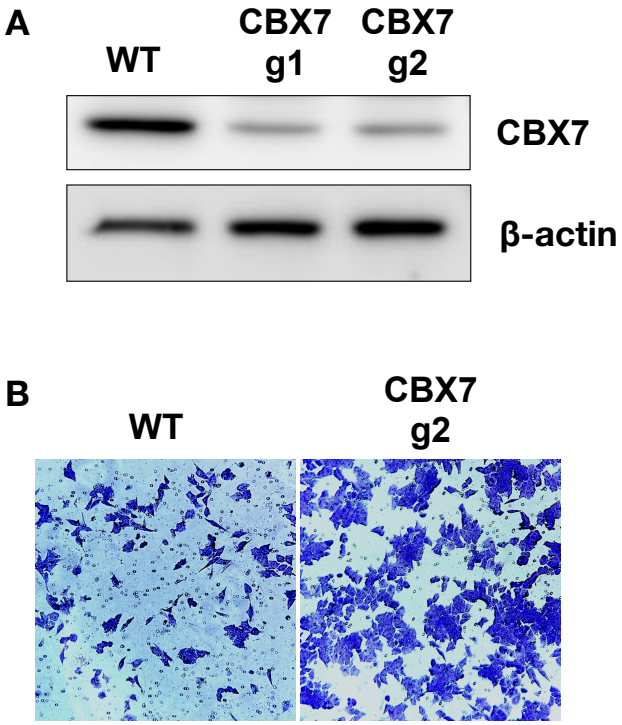

Supplementary Figure 2